CHAPTER 11

Combustion Synthesis of Alloys

Jun Yang, Weimin Liu, Licai Fu, Qinling Bi, Qunji Xue

State Key Laboratory of Solid Lubrication, Lanzhou Institute of Chemical Physics, Chinese Academy of Sciences, Lanzhou 730000, PR China; Tel: +86-931-4968193; Fax: +86-931-8277088. E-mails: jyang@lzb.ac.cn (J Yang), wmliu@lzb.ac.cn (WM Liu)

Abstract: Recently, several groups of alloys have been produced by combustion synthesis. Combustion synthesis of alloys would be an interesting research subject. In this chapter, we will introduce the novel routes to novel materials on combustion synthesis of alloys, containing reactive route design idea, synthesis process, microstructures and properties of the as-prepared alloys.

INTRODUCTION

Alloy is a kind of most common materials in the engineering application fields. Recently, combustion synthesis was successfully employed to prepare alloys. Owing to very low heat release by immediate reaction between element powders, combustion synthesis of alloys must be designed as the highly exothermic reaction system, like thermite reaction, in which case the prepared alloys are usually present in bulk form. At present, the alloys prepared by combustion synthesis mainly include Fe-based alloys and Cu-based alloys etc, such as, Fe-C, Fe-Cu, Fe-Si, Fe-B, Fe-Al, Cu-Al, Cu-Al-Fe, Ni-Al-Cr, Al-Cu-Fe etc alloys. By associating with rapidly solidified technique, the alloys produced by combustion synthesis possess unique metastable microstructures, for example, ultrafine and nano structures or substructures, or quasicrystals, or amorphous, so they usually exhibit superior properties.

DESIGN IDEA ON COMBUSTION SYNTHESIS OF ALLOYS

The combustion reaction between immediate element powders of alloys could not be ignited owing to very low reaction heat release, making use of the aluminothermic reaction with a large amount of exothermic heat to realize the combustion synthesis, then added remainder alloy element to the designed alloy composition, or by combination of the aluminothermic reaction with a weak reaction system such as intermetallics synthesis reaction, the desired alloys could be produced by the combustion synthesis technique when the byproduct Al_2O_3 was separated from the reactive system. Several aluminothermic reaction systems are applied to combustion synthesis of alloys, such as $Fe_2O_3 + Al \rightarrow Fe + Al_2O_3$ (calculated adiabatic temperature T_{ad} about 3800 ℃) [1], $CuO + Al \rightarrow Cu + Al_2O_3$ (T_{ad} about 6500 ℃), $5CrO_3 + Cr_2O_3 + 12Al = 7Cr + 6Al_2O_3$ (T_{ad} about 4100 ℃) [2]. In a word, the alloys by combustion synthesis could be obtained using the large reaction released heat to melt the reaction products and subsequent solidification of the alloy melt, so in most case the alloys are present in bulk form.

COMBUSTION SYNTHESIS OF IRON-BASED ALLOYS

Fe-C Alloy

According to designed component of a Fe-6.5 at.% C alloy ($Fe_2O_3 + 2Al + (0.26/1.87)C = (2/1.87)Fe_{1.87}C_{0.13} + Al_2O_3$), the ferric sesquioxide, aluminum and carbon powders were mixed by a ball mill. The mixed powder was cold-pressed to a copper mould, and an igniter pellet was put on top of the pressed reactant. The chemical reaction of the igniter can be initiated by heating to about 260 ℃, which results in an instantaneous release of a large amount of heat that ignites the aluminothermic reaction. The aluminothermic reaction can be completed in a reactor at about 260 ℃ with 4 MPa argon gas. The processing details have been reported in the literature [1]. The Fe(C) and Al_2O_3 produced are in a very superheated liquid state after reaction. Since liquid Al_2O_3 is immiscible with liquid Fe(C), it is automatically separated and lifts to the top owing to its low density under the high gas pressure [3-5]. The liquid Fe(C) is deposited on the copper mould surface. The resulting $Fe_{1.87}C_{0.13}$ product is about 8 mm in thickness and 100 mm in diameter.

The $Fe_{1.87}C_{0.13}$ material consists of 80-100 nm lamellar eutectic, and has uniform structures from SEM and TEM results (Fig. (1)). The formation of the nanoeutectic microstructure is attributed to three factors [1, 3]. First, the

Maximilian Lackner (ED)

contaminants (Al_2O_3 etc) introduced from reactants and igniter are dissolved in the metallic melt owing to the very high superheating (T_{ad} =3800 ℃), thus there are no heterogeneous nucleation sites for the liquid to crystallize on. Consequently, metallic melt becomes purified and the undercooling degree is greatly increased, which results in a large number of small homogeneous nuclei simultaneously forming during solidification. Second, the diffusion of atoms during nuclei growth is slow owing to the high viscosity of the liquid at the low crystallization onset temperature, resulting the nuclei growth is restricted. Third, the time of nuclei growth is short because of the high cooling rate resulting from the copper substrate quenching. These factors lead to the formation of the observed nanoeutectic in the solidified samples.

The density of the nanostructured $Fe_{1.87}C_{0.13}$ alloy is measured to be 7.60 g/cm^3. The bending strength of the nanostructured $Fe_{1.87}C_{0.13}$ alloy is about 1800 MPa and the yield strength is 1300 MPa. The Vickers microhardness of the nanoeutectic $Fe_{1.87}C_{0.13}$ alloy is 3.85 GPa. After the $Fe_{1.87}C_{0.13}$ alloy is annealed at 800 ℃ in air for 8 hours to obtain a micrometer-scale structure, the hardness and yield strength decrease to 2.2 GPa and 600 MPa, respectively. It indicates the strength of the nanostructured $Fe_{1.87}C_{0.13}$ alloy is much higher than that of the coarse grain counterpart. The nanoeutectic $Fe_{1.87}C_{0.13}$ alloy exhibits good ductility (~40%) in compressive tests. The superior strength originates from that dislocation motion and crack propagation are resisted by the high density of interface of nanoscale lamellar eutectic [1, 3], and the good ductility stems from abundant shear band [1].

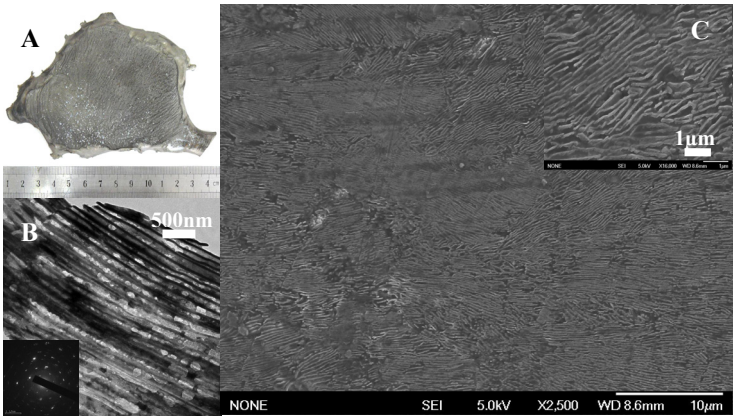

Figure 1: Photograph (A), transmission electron microscope (TEM) image with corresponding selected area electron diffraction (SAED) pattern (B) and scanning electron microscope (SEM) images (C) of the $Fe_{1.87}C_{0.13}$ alloy [1], reproduced with permission of Elsevier.

Fe-B Alloys

Just like the design principle illuminated above, the Fe-B alloys were synthesized by the route of $Fe_2O_3 + Al + B \rightarrow Fe_{100-x}B_x + Al_2O_3$ [6-9]. The prepared processes are similar to that of Fe-C alloy described above. The four component Fe-B alloys (hypoeutectic $Fe_{94.3}B_{5.7}$, eutectic $Fe_{83}B_{17}$, hypereutectic $Fe_{75}B_{25}$, hypereutectic $Fe_{66.7}B_{33.3}$,) have been successfully fabricated [6-9]. The alloys present different dendrite composite ultrafine or nano structures as given in Fig. (2) and Tab. 1. The dendrite phase is tetragonal *t*-Fe_2B and the eutectic phase is γ-Fe and *t*-Fe_2B. The $Fe_{94.3}B_{5.7}$ alloy is a composite structure of micrometer-sized dendrites dispersed in an eutectic matrix. The dendrite trunk thickness is 5 ± 2 μm, and the arm spacing of the dendrite is 10 ± 5 μm. The eutectic colonies distribute uniformly and the size is in the range of 10-20 μm, and the content of the eutectic structure in the $Fe_{94.3}B_{5.7}$ alloy is about 70 vol. % (Fig. 2A). The ultrafine-structured eutectic of the $Fe_{94.3}B_{5.7}$ alloy is relatively disorganized, and the fine α/*t* phases inside the colonies are arranged in an alternating fashion (Fig. 2A inset). The $Fe_{83}B_{17}$ alloy presents a typical all eutectic structure, which is accordant with the Fe-B phase diagram. The size of eutectic colonies is in the range 3-25 μm and the eutectic lamellar spacing is about 30-50 nm (Fig. 2B). The $Fe_{75}B_{25}$ alloy displays a dendrite-ultrafine eutectic composite microstructure with the dendrite volume occupying 10-20 %. The equiaxed eutectic colony size is 8 ± 5 μm, and the dendrite trunk thickness is 5 ± 3 μm and the eutectic lamellar spacing ranges from 150 to 700 nm. The $Fe_{67}B_{33}$ alloy is a line compound according to the equilibrium phase diagram. However, the $Fe_{67}B_{33}$ alloy displays a dendrite-eutectic composite microstructure. It may be attributed to non-equilibrium conditions (the rapid solidification process), which result in the occurrence of the hypereutectic structure. The primary dendrite trunk thickness and spacing are 20 ± 5 and 3 ± 1 μm, respectively. The content of the dendrite in the $Fe_{67}B_{33}$ alloy is above 80 vol.%.

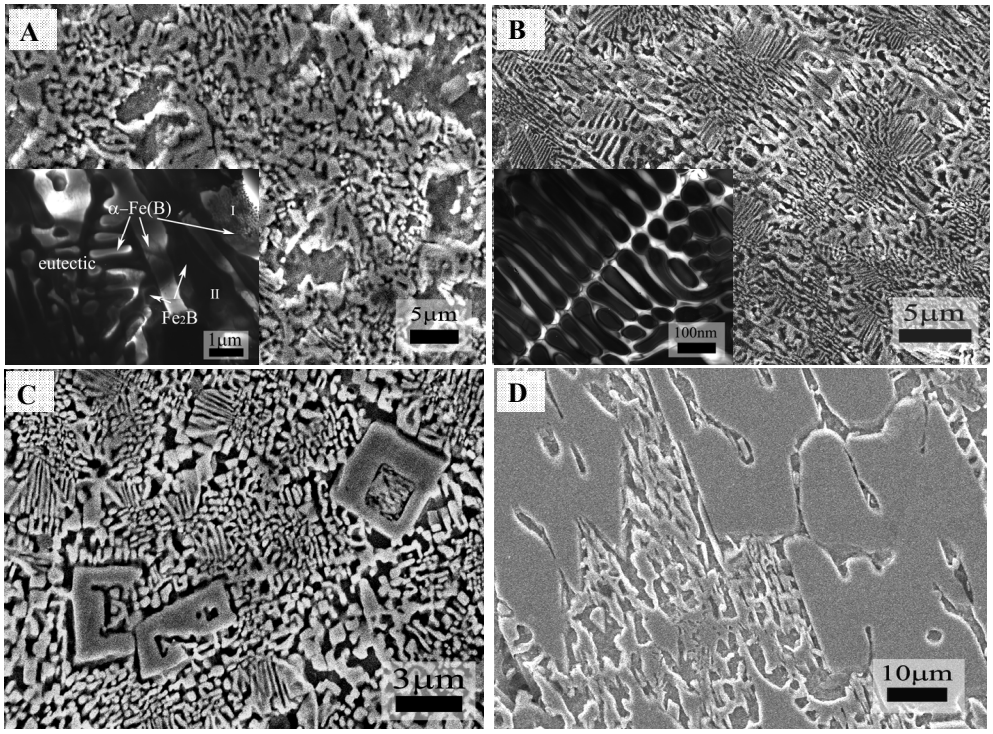

Figure 2: Microstructures of the Fe-B alloys: (A) SEM and TEM (inset) images of hypoeutectic $Fe_{94.3}B_{5.7}$, [8] (b) SEM and TEM (inset) images of eutectic $Fe_{83}B_{17}$, [6] (C) SEM image of hypereutectic $Fe_{75}B_{25}$, [9] (D) SEM image of hypereutectic $Fe_{66.7}B_{33.3}$ [6-9], reproduced with permission of IOP, wiley and Springer.

Table 1: The microstructure morphologies of the Fe-B alloys with different composition.

Alloy	Eutectic colony /μm	Eutectic lamellar spacing/nm	Dendrite trunk thickness /μm	Dendrite spacing /μm	Dendrite fraction /%	Dendrite shape
$Fe_{94.3}B_{5.7}$	10-20	200-600	5 ± 2	10 ± 5	30	Random
$Fe_{83}B_{17}$	3-25	30-50	/	/	0	tetragonal
$Fe_{75}B_{25}$	8 ± 5	150-700	5 ± 3	15 ± 5	10-20	tetragonal
$Fe_{66.7}B_{33.3}$	10-30	/	20 ± 5	3 ± 1	80-90	tetragonal

The nano/ultrafine eutectic of the Fe-B alloys originates from both a high nucleation rate and slow growth of the crystalline nuclei at the solidification of the liquid product. It is similar to the Fe-C alloy. However, the dendrite phase with *t*-Fe_2B of the hypoeutectic $Fe_{94.3}B_{5.7}$ alloy is contrary with the Fe-B phase diagram. It may be related to the growth velocities of Fe and Fe_2B phases. The growth velocity of the Fe_2B phase is always higher than that of the Fe phase as boron content below 15 at.% in the Fe-B alloy under the large undercooling degree [10]. So the effect of solute enrichment at the solid–liquid interface tends to increase the tip radius of the primary Fe_2B. This process will be persisted until the occurrence of stability of solute dendrites. Thus the dendrite phase prefers to *t*-Fe_2B structure rather than α-Fe(B) in the $Fe_{94.3}B_{5.7}$ alloy under the deeply super-cooling degree. Moreover the higher growth velocity of the Fe_2B phase also resulted that the symmetry of lamella eutectic is broke and leads to form a hypereutectic structure (Fe_2B + eutectic) [8].

Compressive test data of the Fe-B alloys are shown in Tab. 2. All of the Fe-B alloys exhibit high strength, and is far from higher than the reported 580 MPa of the coarse crystalline $Fe_{83}B_{17}$ alloy prepared by the traditional technique [6]. The yield strength of Fe-B alloys increases as the dendrite content increase, and the fractured

strain changes only few excepting the $Fe_{66.7}B_{33.3}$ alloy. The obtained large fractured strain and high strength simultaneously is attributed to the dendrite-ultrafine/nano eutectic composite structure. The rotation of the eutectic colonies and dendrites take part in accommodating the shear strain to relieve the concentration stress, result in enhancing the ductility and strength. However, for higher content of dendrite (e.g. above 80%) and coarse dendrite in the eutectic–dendrite composite $Fe_{66.7}B_{33.3}$ alloy, the increase of the stress concentration in the interface can not trigger the coarse dendrite rotate to relieve the stress concentration. So, the catastrophic fracture occurs at the compressive deformation instantaneously.

Table 2: Compressive test data of the different B content Fe-B alloys. [11] (yield strength σ_y, ultimate fracture strength σ_{max}, fracture strain ε_f)

	$Fe_{94.3}B_{5.7}$	$Fe_{83}B_{17}$	$Fe_{75}B_{25}$	$Fe_{66.7}B_{33.3}$
σ_y (MPa)	1430	1090	1430	3400
σ_{max} (MPa)	2600	1260	1650	3400
ε_f (%)	19.8	24.9	20.5	3

Fe-Si alloy

A bulk nanocrystalline $Fe_{88}Si_{12}$ alloy has been produced by adding silicon powders to the aluminothermic reaction ($Fe_2O_3 + 2\ Al + 3/11\ Si = 1/44\ Fe_{88}Si_{12} + Al_2O_3$) [12]. The prepared processes are similar to that of Fe-C alloy described above. The $Fe_{88}Si_{12}$ alloy is composed of the α-Fe(Si) and the Fe_3Si two phases. The $Fe_{88}Si_{12}$ alloy consists of roughly equiaxial grains with a grain size of 5-15 nm and with random orientation. The selected area electron diffraction (SAED) pattern contains two sets of electron diffraction rings, which show that two phases coexist in the bulk nanocrystalline $Fe_{88}Si_{12}$ binary alloy. When the $Fe_{88}Si_{12}$ alloy is cooled down to about 757 ℃, the disordered solid solution *B*2 structure is formed from the *A*2 by unlike-atom pairing of the first nearest neighbors. Then, the microstructure changes in the $Fe_{88}Si_{12}$ binary alloy due to phase separation from *B*2 to ($B2+D0_3$) under 585 ℃ [12]. The nanocrystalline structures were obtained owing to the special processing of combustion synthesis and rapid cooling rate just as described above.

The nanocrystalline $Fe_{88}Si_{12}$ alloy exhibits excellent mechanical performance. The compressive yield strength and ductility reach 1820 MPa and 14.6 %, respectively. These are higher than the reported values (1029 MPa and 3.1 %) of the $Fe_{88}Si_{12}$ prepared by traditional technique [12]. The nanocrystalline $Fe_{88}Si_{12}$ alloy also shows excellent magnet properties, and the coercive force value is approximately 3.6 A/m and saturation magnetization is about 196 emu/g.

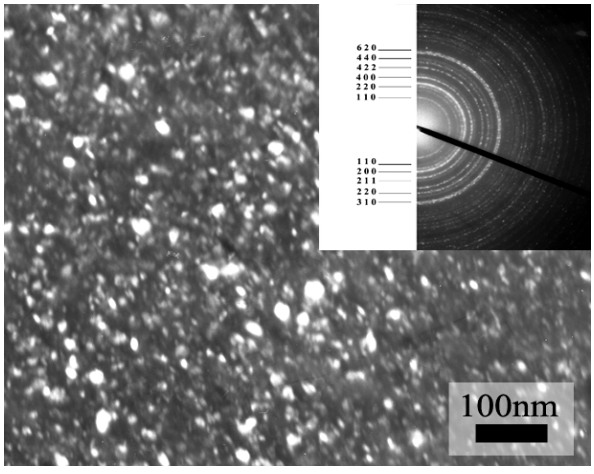

Figure 3: Dark field TEM image and corresponding SAED pattern (inset) of the nanocrystalline $Fe_{88}Si_{12}$ alloy [12], reproduced with permission of IEEE.

Fe-Cu Alloy

The immiscible Fe-Cu alloy system is of particular interest for fundamental research and practical applications [13]. But the Fe-Cu alloys prepared by the conventional solidification techniques have certain limitations. The

large compositional segregation occurs prior to solidification in the Fe-Cu alloys within the immiscible region. A $Fe_{60}Cu_{40}$ alloy has been successfully prepared by the combustion synthesis associating with the rapid solidification technique [14]. Cupric oxide, aluminum and iron powders were weighed and mixed according to the stoichiometry of the design aluminothermic reaction, $6CuO + 4Al + 9Fe = 3/20Fe_{60}Cu_{40} + 2Al_2O_3$, and adiabatic combustion temperature is calculated to be about 4700 ℃, the processing is similar to the Fe-C alloy.

The $Fe_{60}Cu_{40}$ alloy is composed of the dendrites uniformly embedded in the matrix. The dendrite phase and the matrix are Fe(Cu) solid solution (20 at.%Cu) and Cu(Fe) solid solution (43 at.%Fe), respectively. The radius of dendrite trunk is about 3 μm, secondary dendrite arms are with spacing 1-3 μm. The grain size of the matrix is about 30 nm with face-centered cubic (fcc) lattice of Cu-rich phase. The solidification of the Fe-rich and Cu-rich phases is almost simultaneous because of the very high cooling rate resulting from the copper substrate quenching, so the as-prepared $Fe_{60}Cu_{40}$ alloy is no large-scale phase separation. The yield strength of the $Fe_{60}Cu_{40}$ alloy is about 790 MPa, higher than that of commercial polycrystalline Cu-Fe alloys (507 MPa) [14, 15]. A fractured strength of 1100 MPa is obtained in compression test. The alloy displays notable work hardening resulting in a large plastic strain about 30%.

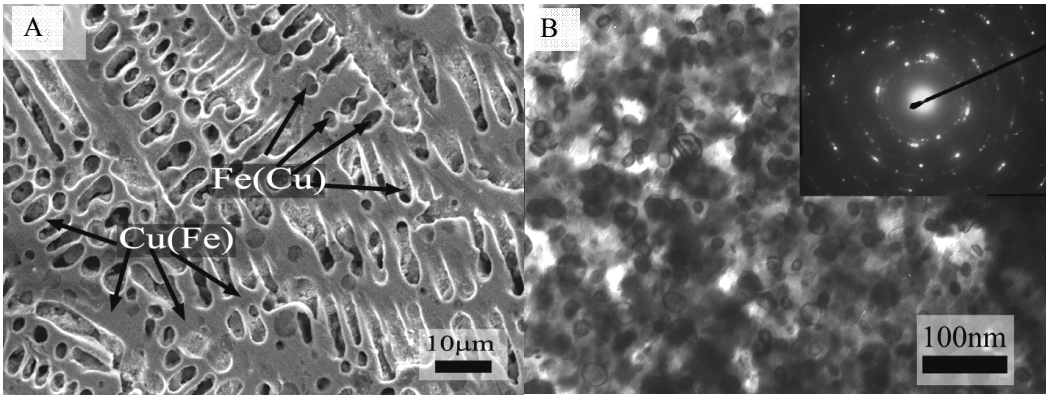

Figure 4: SEM image (A) and TEM image with corresponding SAED pattern (B) of the $Fe_{60}Cu_{40}$ alloy [14], reproduced with permission of Elsevier.

COMBUSTION SYNTHESIS OF COPPER-BASED ALLOYS

A $Cu_{70}Al_{30}$ alloy has been prepared by the reaction ($22Al + 21CuO = 3/10Cu_{70}Al_{30} + 7Al_2O_3$) using combustion synthesis method [16]. The prepared processes are similar to that of Fe-C alloy described above. The $Cu_{70}Al_{30}$ alloy is composed of γ1-Al_4Cu_9 phase and γ1'-$AlCu_3$ martensite phase. The grain size is in the range of 10-30 μm, and the high-dense ultrafine-lamellar substructure embedded in the micro-scaled grains (Fig. 5). The $Cu_{70}Al_{30}$ alloy shows a yield strength of 1080 MPa and a fractured strength of 1440 MPa with a strain of 24% in compression tests. The Vickers microhardness of the $Cu_{70}Al_{30}$ alloy is 6.0 GPa.

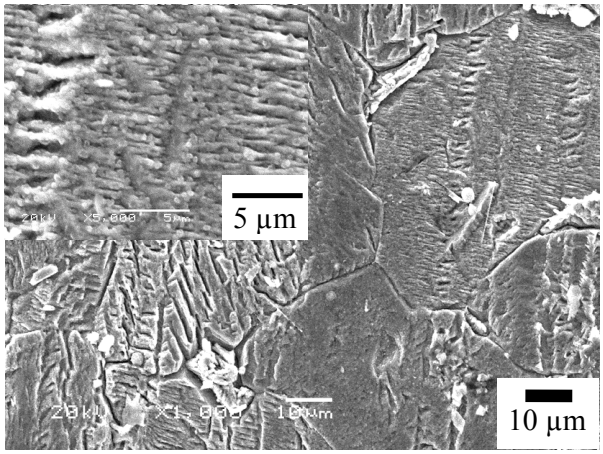

Figure 5: SEM images of the $Cu_{70}Al_{30}$ alloy, inset with high magnification [16].

Four component Cu-Al-Fe ternary alloys, with the λ-$Al_{13}Fe_3$ wear-resistance phase, are produced by the designed reactive route [*3(1-x)CuO + 2(1-x)Al +3x(13Al + 3Fe) → 3Cu$_{1-x}$(Al$_{13}$Fe$_3$)x + (1-x)Al$_2$O$_3$ x=1.0, 1.5, 2.0, 2.5*]. The phase compositions of the alloys are different (Tab. 3). The alloys show different microstructures (Fig. 6). The $Cu_{84}Al_{13}Fe_3$ and $Cu_{76}Al_{19.5}Fe_{4.5}$ alloys consist of equiaxial grains with a grain size of 5–20 nm. The $Cu_{68}Al_{26}Fe_6$ alloy is composed of algae-shape dendrite embedded in martensite matrix with high dense twin and stack fault. The $Cu_{60}Al_{32.5}Fe_{7.5}$ alloy comprises the nano-scaled dendrite. The Cu-Al-Fe alloys exhibit different mechanical properties. The strength and hardness increase with the increase of the nominal content of the λ-$Al_{13}Fe_3$ wear-resistance phase. [16]

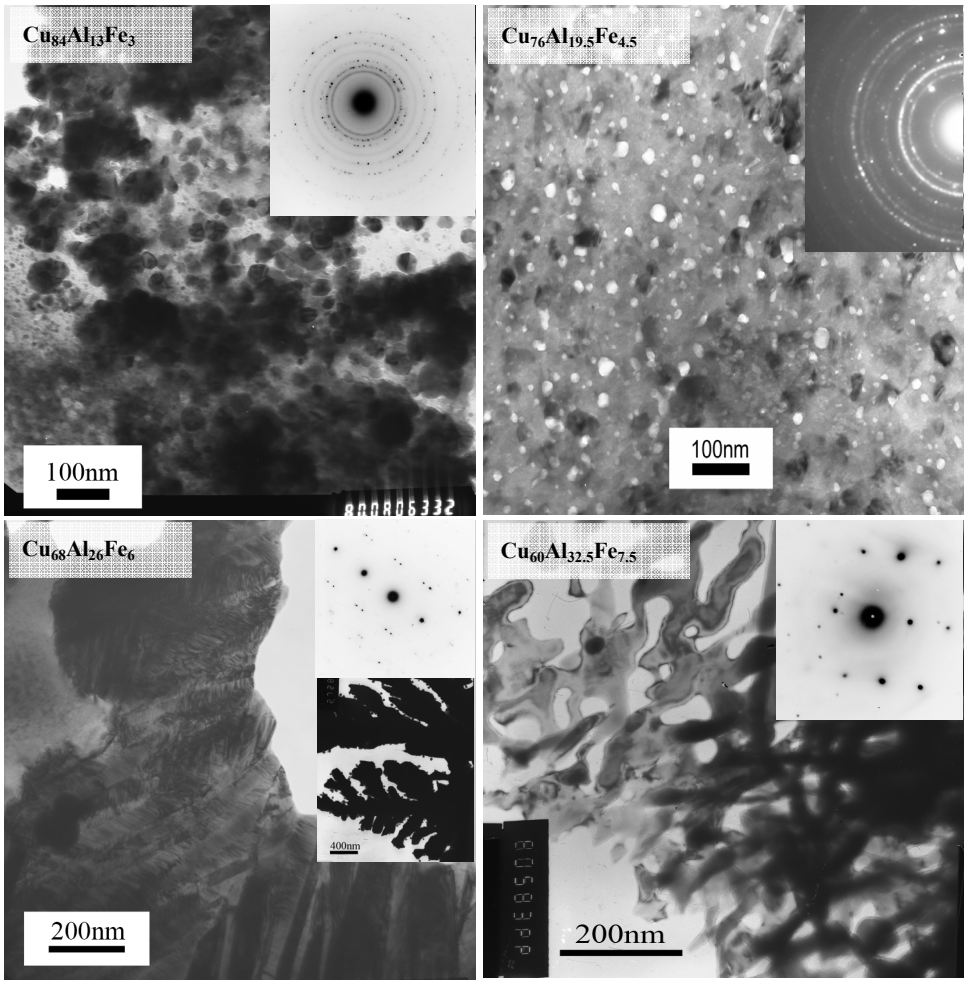

Figure 6: TEM images and corresponding SAED patterns (inset) of the Cu-Al-Fe alloys. [16]

Table 3: Phase composition in the Cu-Al-Fe alloys.

Alloy	Phase composition	Matrix phases
$Cu_{84}Al_{13}Fe_3$	α(3R)	α(3R)
$Cu_{76}Al_{19.5}Fe_{4.5}$	α + β_1' + λ ($Al_{13}Fe_3$)	α(3R)+ β_1' (M18R)
$Cu_{68}Al_{26}Fe_6$	β1' + γ_1+ λ ($Al_{13}Fe_3$)	β_1' (M18R) + γ_1(Al_4Cu_9)
$Cu_{60}Al_{32.5}Fe_{7.5}$	γ_1+ ε(Al_2Cu_3) + β-Al(Cu, Fe)	γ_1(Al_4Cu_9)

α: fcc-Cu, β_1': M18R martensite phase, γ_1: complex cubic phase, ε: hexagonal phase

Table 4: Compressive strength and hardness value of the Cu-Al-Fe alloys. Yield stress σ_y, ultimate compression stress σ_{max}, plastic strain ε_p and elastic strain ε_e.

Composition (at.%)	σ_y (MPa)	σ_{max} (MPa)	ε_p (%)	ε_e (%)	Hv (GPa)
$Cu_{84}Al_{13}Fe_3$	238	/	/	/	1.7
$Cu_{76}Al_{19.5}Fe_{4.5}$	591	1336	39.3	10	2.1
$Cu_{68}Al_{26}Fe_6$	1150	1669	15.6	15	5.2
$Cu_{60}Al_{32.5}Fe_{7.5}$	1407	1604	2	15	7.0

COMBUSTION SYNTHESIS OTHER ALLOYS

Al-Cu-Fe Quasicrystalline Alloy

Quasicrystalline (QC) materials have attracted considerable attention owing to their excellent physical, chemical, mechanical and tribological properties. The Al-Cu-Fe QC materials are with the thermodynamic stability, non-toxicity and low costs, so they possess great potentials for practical applications in the following areas including thermal barrier coatings, low-friction wear-resistant coatings, composite biomaterials, catalysts as well as reinforcement phases / fillers for composite materials [17, 18].

An $Al_{62}Cu_{25.5}Fe_{12.5}$ alloy powder has been fabricated by the designed reaction system (*79Al + 25.5CuO + 12.5Fe = $Al_{62}Cu_{25.5}Fe_{12.5}$ + 8.5Al_2O_3*, T_{ad} about 2900 ℃) using combustion synthesis [19]. The prepared processes of the bulk samples are similar to that of Fe-C alloy described above, then the brittle bulk samples are pulverized to the powder samples by ball milling. The Al-Cu-Fe alloy consists of icosahedral quasicrystalline (IQC) ψ-$Al_{65}Cu_{20}Fe_{15}$, cubic β-Al (Cu, Fe) and a spot of φ-$Al_{10}Cu_{10}Fe$ phases (Fig. 7), and the volume fractions of the IQC, the β and the φ phases are calculated from XRD results to be about 68, 30 and 2 %, respectively. The grain size of the quasicrystalline sample is in the range of 50-200 nm (Fig. 7), which is smaller than that of the $Al_{65}Cu_{20}Fe_{15}$ coating prepared by electron beam physical vapor deposition technique (200-400 nm) [20]. The IQC phase is formed owing its low interfacial energy in the liquid melts. The formation of ultrafine grains is attributed to the copious nucleation and slow growth rate induced by rapid quenching.

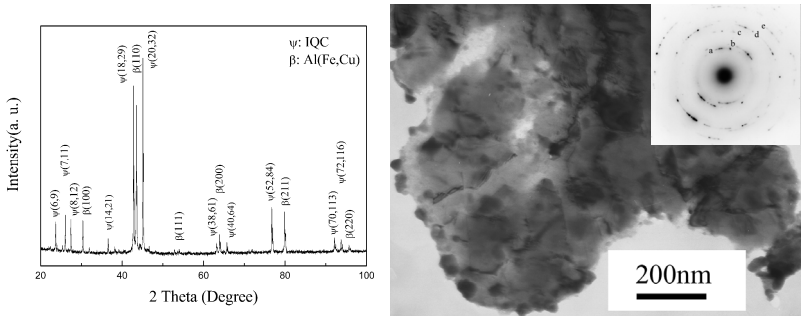

Figure 7: The XRD pattern and TEM image and corresponding SAED pattern of the Al-Cu-Fe quasicrystal alloy [19], reproduced with permission of Elsevier.

Ni-Al-Cr Alloy

Making use of the combustion synthesis technique, a bulk $Ni_{64}Al_{21}Cr_{15}$ alloy has been produced by designing the reaction systems to combine the aluminothermic reaction (*5CrO_3 + Cr_2O_3 + 12Al = 7Cr + 6Al_2O_3*) with the weak exothermic reaction (*3Ni + Al = Ni_3Al*, T_{ad} about 1400 ℃) [21]. The prepared process of the $Ni_{64}Al_{21}Cr_{15}$ alloy is similar to that of Fe-C alloy described above. The $Ni_{64}Al_{21}Cr_{15}$ alloy is composed of the γ'-Ni_3Al(Cr) and γ-Ni(Cr) phases by XRD analysis. The $Ni_{64}Al_{21}Cr_{15}$ alloy presents a composite structure of micrometer sized dendrites dispersed in the matrix, and the dendrite volume occupies about 40 %. The matrix mainly consists of the uniform nano square grains with the sizes in the range of 80-120 nm (Fig. 8). The dendrites comprise the 100-300 nm thickness of lamellar structures embedded high-dense twins with the thickness ranged from 3-20 nm (Fig. 8) [21]. The $Ni_{64}Al_{21}Cr_{15}$ alloy exhibits coexisting high strength (fractured strength of 2300 MPa) and high

ductility (26%) in the compressive testing.

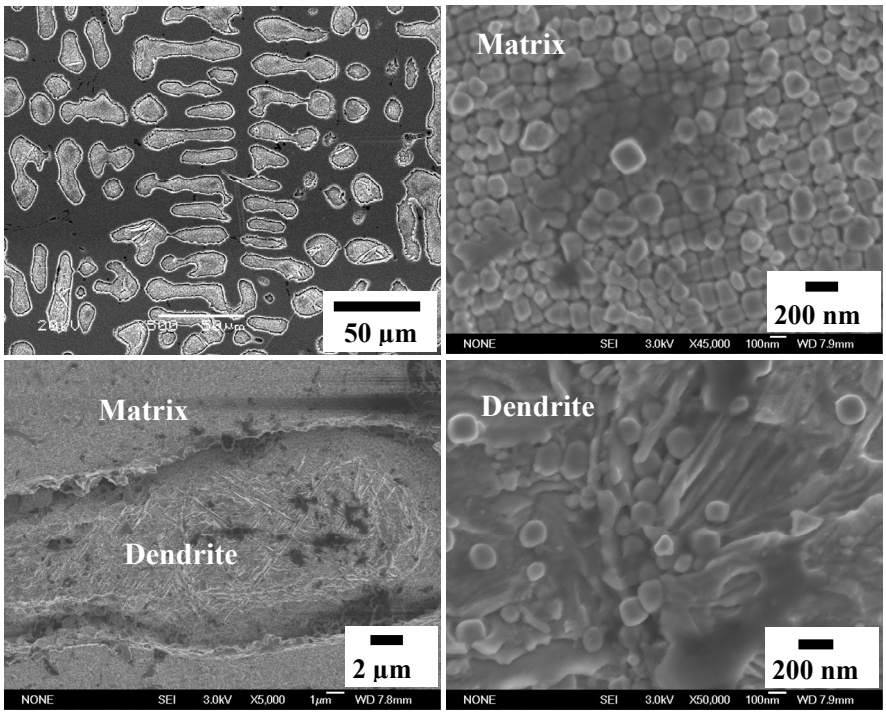

Figure 8: SEM images of the $Ni_{0.64}Al_{0.21}Cr_{0.15}$ alloy. [21]

SUMMARY

Making use of combustion synthesis, alloys have been produced by designing the highly exothermic reaction systems. The alloys produced by CS method usually show special microstructures, such as ultrafined and nano structures or sub-structures, and exhibit superior properties owing to present special nonequilibrium processes. It is important in science and technology to develop the routs on CS of alloys, in particular nanostructured, amorphous, immiscible and high melting point alloys.

ACKNOWLEDGEMENTS

This work was supported by the National Natural Science Foundation of China (50801064) and the National 973 project of China (2007CB607601) and the Innovation Group Foundation from NSFC (50721062). The authors also thank all the coworkers, Prof. P.Q. La, Dr. L.J. Li, Dr. J.Q. Ma, Dr. L. Wang and Dr. Y.H. Kang.

REFERENCES

[1] Yang J, Ma JQ, Liu WM, Bi QL, Xue QJ. Large-scale Fe–C nanoeutectic alloy prepared by a self-propagating high-temperature synthesis casting route. Scripta Mater 2008; 58: 1074-1077.

[2] Bi QL, La PQ, Liu WM, Xue QJ. Microstructure and properties of Ni_3Si alloyed with Cr fabricated by self-propagating high-temperature synthesis casting route. Metall. Mater. Trans. A 2005; 36: 1301-1307.

[3] La PQ, Yang J, Cockayne DJH, Liu WM, Xue QJ. Bulk nanocrystalline Fe_3Al-based material prepared by aluminothermic reaction. Adv Mater 2006; 18(6): 733-737.

[4] Yang J, La PQ, Liu WM, Hao Y. Fe_3Al-$Fe_3AlC_{0.5}$ composites fabricated by self-propagating high temperature synthesis casting. Mater Sci Eng A 2004; 382: 8-14.

[5] Ma JQ, Yang JQ, Bi QL, Liu WM. Preparation of an ultrafine-grained Fe-40Al intermetallic compound. Acta Metallurgica Sinica (English Letters), accepted.

[6] Fu LC, Yang J, Bi QL, Li LJ, Liu WM. Microstructure and mechanical behavior of nano-eutectic $Fe_{83}B_{17}$ alloy prepared by a self-propagating high temperature synthesis combining rapid solidification. J Phys D: Appl Phys 2008; 41: 235401.

[7] Fu LC, Yang J, Bi QL, Liu WM. Ultrafine eutectic-dendrite composite bulk Fe-B alloy with enhanced ductility. Mater Trans 2009;50 :2108-2110.
[8] Fu LC, Yang J, Bi QL, Li LJ, Liu WM. Nanostructured hypoeutectic Fe-B alloy prepared by a self-propagating high temperature synthesis combining a rapid cooling technique. Nanoscale Res Lett 2009; 4: 11-16.
[9] Fu LC, Yang J, Bi QL, Liu WM. Enhanced ductility of dendrite-ultrafine eutectic composite Fe_3B alloy prepared by a self-propagating high temperature synthesis. Adv Eng Mater 2009; 11: 194-197.
[10] Palumbo M, Cacciamani G, Bosco E, Baricco M. Driving forces for crystal nucleation in Fe-B liquid and amorphous alloys. Intermetallics 2003; 11: 1293-1299.
[11] Fu LC. Properties of bulk nanostructured Fe-Si and Fe-B alloys prepared by combustion synthesis. Ph.D. Thesis, Chinese Academy of Sciences.
[12] Fu LC, Yang J, Bi QL, Ma JQ, Liu WM. Combustion synthesis and characterization of bulk nanostructured $Fe_{88}Si_{12}$ alloy. IEEE Trans Nanotechnology 2009, accepted.
[13] Ma E. Alloys created between immiscible elements. Prog. Mater. Sci. 2005; 50: 413-509.
[14] Fu LC, Yang J, Bi QL, Liu WM. Combustion synthesis immiscible nanostructured Fe-Cu alloy. J Alloys Compd 2009; 482, L22-L24.
[15] Kakisawa H, Minagawa K, Halada K. Tensile behavior change depending on the microstructure of a Fe-Cu alloy produced from rapidly solidified powder. Mater. Sci. Eng. A 2003; 340: 175-180.
[16] Li LJ. Fabrication, microstructure and properties of bulk nano-structured copper alloys. Ph.D. Thesis, Chinese Academy of Sciences.
[17] Inoue A. Amorphous, nanoquasicrystalline and nanocrystalline alloys in Al-based systems. Prog Mater Sci 1998; 43: 365-520.
[18] Shechtman D, Blech I, Gratias D, Chan JW. Metallic phase with long-range orientational order and no translational symmetry. Phys Rev Lett 1984; 53: 1951.
[19] Li LJ, Bi QL, Yang J, *et al*. Large-scale synthesis of Al–Cu–Fe submicron quasicrystals. Scripta Mater 2008; 59: 587-590.
[20] Milman YV, Lotsko DV, Dub SN *et al*. Mechanical properties of quasicrystalline Al-Cu-Fe coatings with submicron-sized grains. Surf Coat Tech 2007; 201: 5937-5943.
[21] Ma JQ. Microstructures and properties of bulk nanocrystalline Ni_3Al based materials prepared by combustion synthesis casting. MD. Thesis, Chinese Academy of Sciences.